RSC Advances

PAPER

View Article Online
View Journal | View Issue

Cite this: *RSC Adv.*, 2016, **6**, 22411

Strange critical behaviors of ferromagnetic to paramagnetic transition in $La_{0.5}Ca_{0.5}MnO_3$ nanowires bundles

Fei Fang,[a] Bo Hong,*[a] Langsheng Ling,[b] Jingcai Xu,[a] Hongxiao Jin,[a] Dingfeng Jin,[a] Xiaoling Peng,[a] Jing Li,[a] Yanting Yang[a] and Xinqing Wang[a]

Received 8th January 2016
Accepted 15th February 2016

DOI: 10.1039/c6ra00650g

www.rsc.org/advances

Highly ordered $La_{0.5}Ca_{0.5}MnO_3$ nanowires bundles are synthesized using mesoporous SBA-15 silica as the hard template. The magnetic properties and critical behaviors of the ferromagnetic–paramagnetic (FM–PM) phase transition of the $La_{0.5}Ca_{0.5}MnO_3$ nanowires bundles are investigated through isothermal magnetization methods. The calculated results show that the FM–PM transition is second order and the magnetic interaction has some deviations from the mean-field model. Though the obtained critical parameters of $\beta = 0.596 \pm 0.009$, $\gamma = 1.131 \pm 0.008$ and $\delta = 2.99 \pm 0.05$ follow the Widom scaling relation $\delta = 1 + \gamma/\beta$ and the single scaling equation $M(H,|\varepsilon|) = \varepsilon^{\beta} f_{\pm}(H/|\varepsilon|^{\beta+\gamma})$, the critical exponents do not obey the magnetization entropy scaling theory, indicating that the nanometer-size effect play a significant role on the magnetic phase transition and magnetic entropy for $La_{0.5}Ca_{0.5}MnO_3$ nanowires bundles.

Introduction

Mixed-valent perovskite manganite compounds $RE_{1-x}AE_xMnO_3$ (RE = trivalent rare earth ions, such as La, Pr, Nd, Sm, *etc.* and AE = divalent alkaline earth ions, such as Sr, Ca, Ba and Pb *etc.*) have attracted much attention due to their extraordinary magnetic and electronic properties,[1,2] as well as potential applications, such as cathodes for solid oxide fuel cells (SOFC),[3,4] oxidation catalysts[5] and magnetic sensors.[6] Compared with transition metal groups of iron, nickel and cobalt which also have pretty large saturation magnetization,[7–10] the perovskite oxides show peculiar physical properties such as colossal magnetoresistance (CMR) accompanied with FM–PM transition. A prominent feature of these materials is an insulation–metallic transition associated with ferromagnetic–paramagnetic transition. The double exchange (DE) effect in which e_g electrons transfer between adjacent Mn^{3+} and Mn^{4+} ions and the Jahn–Teller effect were used to understand FM–PM transition in the manganites.[1,11] In recent years, nano-structured perovskites have been investigated for their amazing chemical and physical properties such as high catalytic activities,[12,13] electrochemical performance[14] and unique magnetism[15–19] which are different from their bulk counterparts. For nano-scale magnetic materials, the size effect becomes more significant because the magnetic disorder at surface and interface caused by defects, broken bonds, *etc.* can change of the magnetic properties of the system.[20] In previous works, many attempts have been made to investigate magnetic nanoparticles due to the interesting size effects and surface magnetism.[21,22] Several works showed that nanoscale $La_{1-x}AE_xMnO_3$ have two peculiar features: loss of charge orbital order and strengthen of FM order.[15,23,24] An earlier study on $La_{0.9}Sr_{0.1}MnO_3$ samples by H. Baaziz *et al.*[25] has shown that the size reduction had strong impact on the critical behaviors. For $La_{0.9}Sr_{0.1}MnO_3$ nanoparticles with size of 44.98 nm, the critical exponent β (associated with spontaneous magnetization M_s) is a bit higher than the mean-field model value and γ (associated with the initial magnetic susceptibility χ_0) is similar to the 3D Heisenberg model value. These phenomena were attributed to the smaller grain size and the larger surface effects. To understand the unique magnetic behavior, it is necessary to study the details of magnetic phase transition mechanism in nano-structure perovskites. For Ca^{2+} doped manganites, the order of ferromagnetic–paramagnetic phase transition may be related to the colossal magneto resistance (CMR) near Curie temperature (T_c).[26,27] It has been reported the FM–PM phase transition for $La_{1-x}Ca_xMnO_3$ ($x = 0.33$) is first order due to strong electron–phonon coupling and intrinsic inhomogeneity.[28] Furthermore, the FM–PM phase transition of $La_{1-x}Ca_xMnO_3$ ($x = 0.4$) is in good agreement with tricritical point values setting a boundary between first order ($x < 0.4$) and second order ($x > 0.4$) within the ferromagnetic range ($0.2 < x < 0.5$).[28] For $La_{1-x}Ca_xMnO_3$ ($x = 0.2$), the FM–PM transition is second order corresponding to Heisenberg model describing short-range interaction.[29] For

[a]*Zhejiang Province Key Laboratory of Magnetism, College of Materials Science and Engineering, China Jiliang University, Hangzhou, 310018, China. E-mail: bohong@cjlu.edu.cn; bongbo@mail.ustc.edu.cn; Fax: +86-571-8767-6175; Tel: +86-571-8767-6175*

[b]*High Magnetic Field Laboratory, Chinese Academy of Sciences, Hefei, 230031, China*

single crystal $La_{1-x}Ca_xMnO_3$ ($x \approx 0.25$), Belevtsev identified the FM–PM phase transition is first order.[30] However, Zainullina estimated the FM–PM transition should be first order below 205 K while second order above 205 K.[31] The $La_{1-x}Sr_xMnO_3$ also showed various FM–PM transition behaviors with different degrees of Sr doped.[32,33] M. Hazzez *et al.* calculated the critical exponents of bulk $La_{0.5}Sr_{0.5}MnO_3$ and showed that the transition is second-order corresponding to the mean-field model with critical exponents $\beta = 0.507$ and $\gamma = 1.107$ which dominated by long-range interaction around T_c.[33] Since the FM–PM phase transition has a strong correlation with the level of divalent alkaline earth doping, it is important to focus on the FM–PM transition order of $La_{1-x}Ca_xMnO_3$ ($x = 0.5$). In general, half doped manganites show very interesting properties such as charge and orbital order, phase segregation and high CMR values.[34,35] In the case of bulk $La_{0.5}Ca_{0.5}MnO_3$, it's a paramagnetic insulator at high temperature, and becomes ferromagnetic upon cooling ($T_c \sim 225$ K) and then antiferromagnetic at $T_N \sim 155$ K.[35] The polycrystalline sample $La_{0.5}Ca_{0.5}MnO_3$ exhibits double transition $T_c \sim 230$ K and $T_N \sim 170$ K.[36] However, there are few reports focusing on the FM–PM phase transition of nano-sized $La_{0.5}Ca_{0.5}MnO_3$. Several methods have been reported for synthesising $La_{0.5}Ca_{0.5}MnO_3$ nanomaterials, but no reports have focused on the hard template method.[15,37] In this paper, we synthesized $La_{0.5}Ca_{0.5}MnO_3$ nanowires bundles by hard template method using mesoporous silica SBA-15. Furthermore, the static magnetization were measured around Curie temperature (T_c) and the critical properties were investigated through isothermal magnetization methods.

Experimental details

Preparation of $La_{0.5}Ca_{0.5}MnO_3$ nanowires bundles

The mesoporous silica SBA-15 was synthesized according to the procedure described in the previous reports.[38] SBA-15 is a well ordered one-dimensional hexagonal silica-block copolymer mesophase and the pore size can be controlled. 5.85 g of the surfactants P123 (poly(ethyleneglycol)–poly(propylene glycol)–poly(ethylene glycol)) as the soft template was dissolved in the mixture of 94.235 g of HCl (2 mol) and deionized water with vigorously stirred for 2 h. And then a total of 13.4 ml of tetraethyl orthosilicate (TEOS, 98%, Aldrich) as the silicon source was added. After stirred for 5 min and aged at 45 °C for 24 h, the mixture was transferred into a Teflon-lined autoclave, then treated hydrothermally at 130 °C for 24 h. The product was filtered and washed with deionized water and ethyl alcohol after cooling to room temperature naturally. The final powder was calcined at 550 °C for 6 h to remove the P123.

To synthesize ordered $La_{0.5}Ca_{0.5}MnO_3$ nanowires bundles, 0.0025 mol $La(NO_3)_3 \cdot 6H_2O$, 0.0025 mol $Ca(NO_3)_2 \cdot 4H_2O$, 0.01 mol 50 wt% $Mn(NO_3)_2$ solution and 0.01 mol citric acid were dissolved in the mixture of 30 ml ethanol and 10 ml distilled water with continuous stirring, followed by the addition of 2 g SBA-15. Then the mixtures were stirred at 60 °C until dry powders were obtained. The samples were then heated to 300 °C from room temperature (1 °C min^{-1}) followed a calcination at 300 °C for 6 h to pyrolyze the precursor. The obtained materials were re-impregnated by 0.00125 mol $La(NO_3)_3 \cdot 6H_2O$, 0.00125 mol $Ca(NO_3)_2 \cdot 4H_2O$, 0.005 mol 50 wt% $Mn(NO_3)_2$ solution and 0.005 mol citric acid in the mixture of 30 ml ethanol and 10 ml distilled water at 60 °C and stirred to dry. Then the soaked samples were heated to 650 °C under the heating rate of 1 °C min^{-1} from room temperature and calcined at 650 °C for 6 h. To remove the template SBA-15, the obtained samples were treated in a 2 M NaOH solution at 80 °C for 0.5 h, followed by washing with distilled water and ethanol several times. The final obtained $La_{0.5}Ca_{0.5}MnO_3$ nanowires bundles were copied the pore structure of the hard template SBA-15.

Characterization

Phase formation and crystallinity of the obtained $La_{0.5}Ca_{0.5}MnO_3$ nanowires bundles were characterized by X-ray diffraction (XRD, DX-2700, Cu target, $\lambda = 0.154$ nm, $U = 40$ kV, step was 0.02°). Nitrogen physisorption experiments were measured at 77 K on a Micrometrics ASAP 2020 surface area and porosity analyzer. Specific surface areas of the powders was estimated from the relative pressure range of 0.06 to 0.2. The morphologies of the template SBA-15 and the prepared $La_{0.5}Ca_{0.5}MnO_3$ nanowires bundles were observed by scanning electron microscope (SEM). The magnetic properties were studied by Superconducting Quantum Interference Device (SQUID) MPMS.

Results and discussion

The highly ordered 1D mesoporous structure in SBA-15 is observed by SEM (Fig. 1a). The diameter of the cages is measured to be about 10.8 nm from the SBA-15 SEM image, in good accordance with the pore diameter distribution graph which is inserted in Fig. 1b. Nitrogen sorption isotherm (Fig. 1b) for the SBA-15 samples shows a type IV and a large H1 hysteresis loop, indicating the typical mesoporous structure of the template.

X-ray diffraction (XRD) pattern (Fig. 2) shows that the $La_{0.5}Ca_{0.5}MnO_3$ nanowires bundles are single phase and can be indexed on basis of an orthorhombic cell with space group *pnma*.[39] No peaks of impurities are observed. All the diffraction peaks are broad corresponding to the nanocrystals structure.

The nanostructure and morphology of $La_{0.5}Ca_{0.5}MnO_3$ were analyzed by scanning electron microscopy (SEM) as shown in Fig. 3a, in which the crossing section shows ordered arrangement and uniform nanowires structure, indicating the obtained samples reproduced the pore structure of SBA-15 successfully. This unique 1D nanowires bundles structure also leads to the high specific surface area 132.45 $m^2 g^{-1}$ (analyzed by nitrogen physisorption). Fig. 3b shows N_2 adsorption–desorption isotherm of the $La_{0.5}Ca_{0.5}MnO_3$ nanowires bundles and a type IV isotherm with a clear H1 type hysteretic loop is observed. It is a characteristic of mesoporous metal oxide materials, further indicating that the samples templated from molecular sieve have replicated the template pore structure successfully.

Shown in Fig. 4 is the temperature dependence of magnetization (M–T) under applied field of 100 Oe. All data were taken in the warming run after zero-field cooling (ZFC, solid circles)

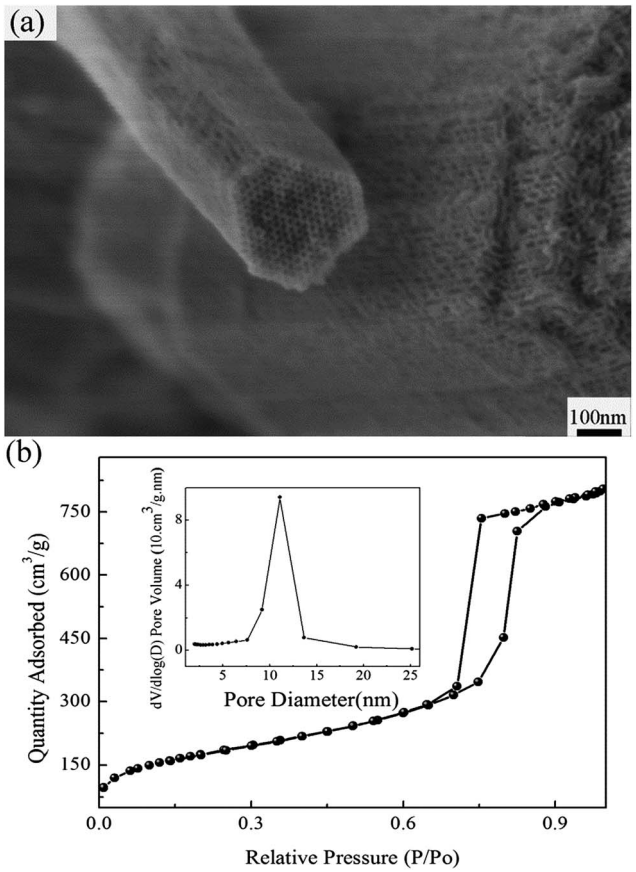

Fig. 1 (a) SEM image of the hard template SBA-15. (b) Nitrogen sorption isotherms of SBA-15, the inserted picture is pore diameter distribution graph.

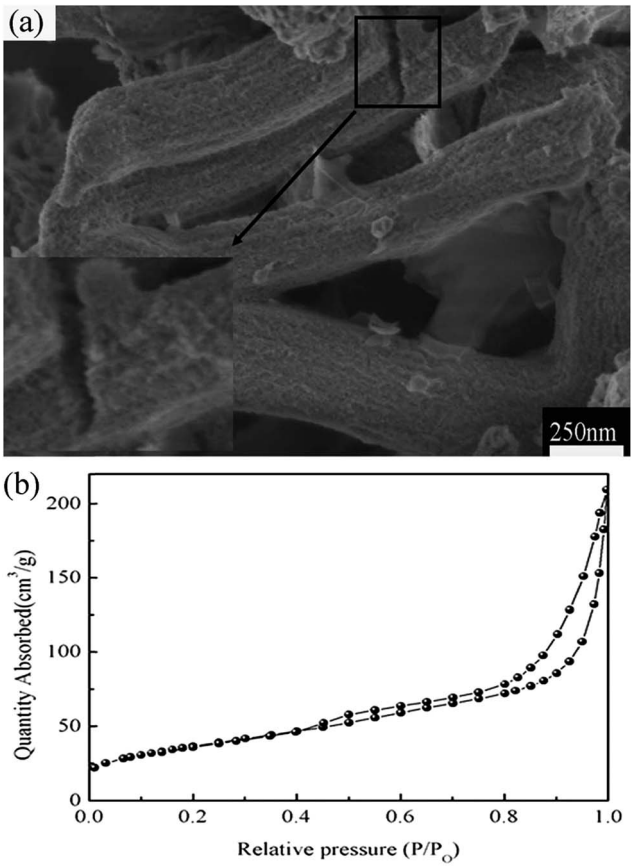

Fig. 3 (a) SEM image of the prepared $La_{0.5}Ca_{0.5}MnO_3$. (b) Nitrogen sorption isotherms of $La_{0.5}Ca_{0.5}MnO_3$ nanowires bundles.

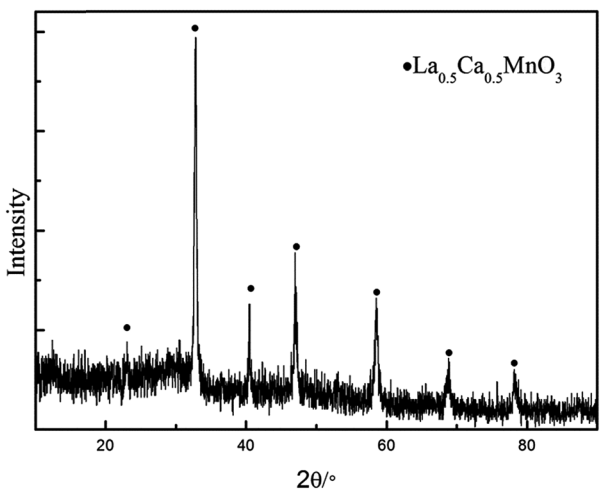

Fig. 2 XRD pattern of $La_{0.5}Ca_{0.5}MnO_3$ nanowires bundles templated from SBA-15.

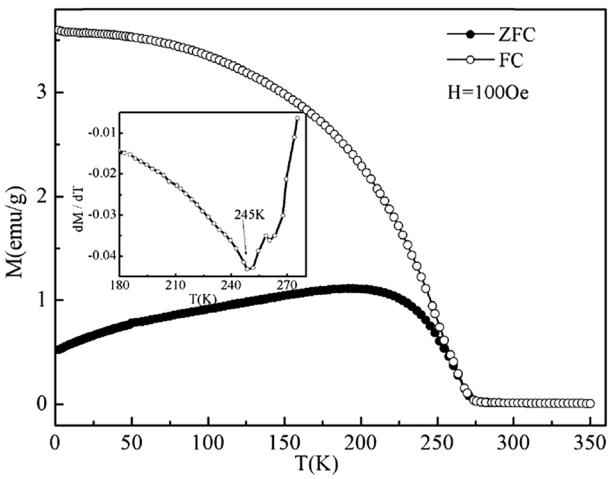

Fig. 4 Temperature dependence of magnetization for $La_{0.5}Ca_{0.5}MnO_3$ nanowires bundles measured at a field of 100 Oe. The insert depicts dM/dT *vs.* temperature curves for this material.

and field cooling (FC, open circle), respectively. An FM–PM transition occurs at 245 K, which was defined by the minimum in the dM/dT (insert in Fig. 4). A considerable divergence between the ZFC and FC curves implies the existence of surface magnetic disorders. Generally, for half doped $La_{1-x}Ca_xMnO_3$, the charge ordering state and antiferromagnetic phase are ubiquitous. However, these characteristics are not detected in this nanowires bundles system, indicating the charge ordering state maybe destroyed due to nanometer size effect. In order to deeply clarify the nanometer size effect on the magnetic phase

transition, we further investigated the critical behaviors which can be described by the critical exponents.

In common, the critical exponents are deduced by the fitting values obtained from the Arrott–Noakes equation of state,[40] $(H/M)^{1/\gamma} = (T - T_c)/T_c + (M/M_1)^{1/\beta}$ where M_1 refers to material constant. The Arrott plots of $M^{1/\beta}$ *vs.* $(H/M)^{1/\gamma}$ obtained under different temperatures should reveal a series of parallel straight lines and the line should pass through the origin when $T = T_c$. Generally, some different theoretical models were firstly used to construct tentative Arrott plots and then the best one was chosen to be initial Arrott plot for fitting data. In order to obtain correct values of β and γ, four different kinds of trial exponents including tricritical mean-field theory ($\beta = 0.25$, $\gamma = 1$), 3D Heisenberg model ($\beta = 0.365$, $\gamma = 1.336$), 3D Ising model ($\beta = 0.325$, $\gamma = 1.24$), and mean-field theory ($\beta = 0.5$, $\gamma = 1$), were used to make the regular Arrott plots (Fig. 5). As shown in Fig. 5d, only mean-field theory is suitable approximate for the materials. The M^2 *vs.* H/M ($\beta = 0.5$, $\gamma = 1$) curves reveal an analogous linear behavior at $T = 238$ K and the line should just pass through the origin which determines the T_c approach to 238 K. However, all the lines are not completely parallel to each other and upward curvature, indicating the M^2 *vs.* H/M with in the framework of mean-field needs to be modified.

According to the criterion proposed by Banerjee,[41] the positive slope of M^2 *vs.* H/M lines corresponds to the second-order transition while the negative slope corresponds to the first-order transition. It is obvious that, in the present system, the positive slope of M^2 *vs.* H/M indicates the FM to PM transition to be of the second order.

According to the scaling hypothesis,[42] the critical behaviors of a magnetic system, which shows a second order magnetic phase transition near the curie point, were characterized through a series of critical exponents. The mathematical definition of the exponents from magnetization measurement can be described as

$$M_s(T) = M_0(-\varepsilon)^{\beta} \quad (1)$$

$$\chi_0(T)^{-1} = (h_0/M_0)\varepsilon^{\gamma},\ \varepsilon > 0 \quad (2)$$

$$M = DH^{1/\delta},\ \varepsilon = 0,\ T = T_c \quad (3)$$

where $\varepsilon = (T - T_c)/T_c$ is the reduced temperature, h_0, M_0 and D are critical amplitudes. The parameters β, γ and δ (associated with T_c) are the critical exponents.

In order to obtain the accurate critical exponents, it is necessary to use some tentative exponents to construct a new Arrott plot and then fit the data of the liner part. As shown in Fig. 5d, M_s and χ_0^{-1} can be obtained by liner extrapolation from the high-field region to the intercept. These values as functions of temperature, χ_0^{-1} *vs.* T and $M_s(T,0)$ *vs.* T, are plotted in Fig. 6. According to the eqn (1) and (2), the values can be fitted to two continuous curves, then the modified critical parameter $\beta = 0.596 \pm 0.009$ with $T_c = 238.6 \pm 0.5$ K, and $\gamma = 1.131 \pm 0.008$ with $T_c = 237.5 \pm 0.6$ K can be obtained.

Fig. 7a shows the Arrott plot with modified exponents. A series of parallel lines are obtained in the high region of 1–6 T as

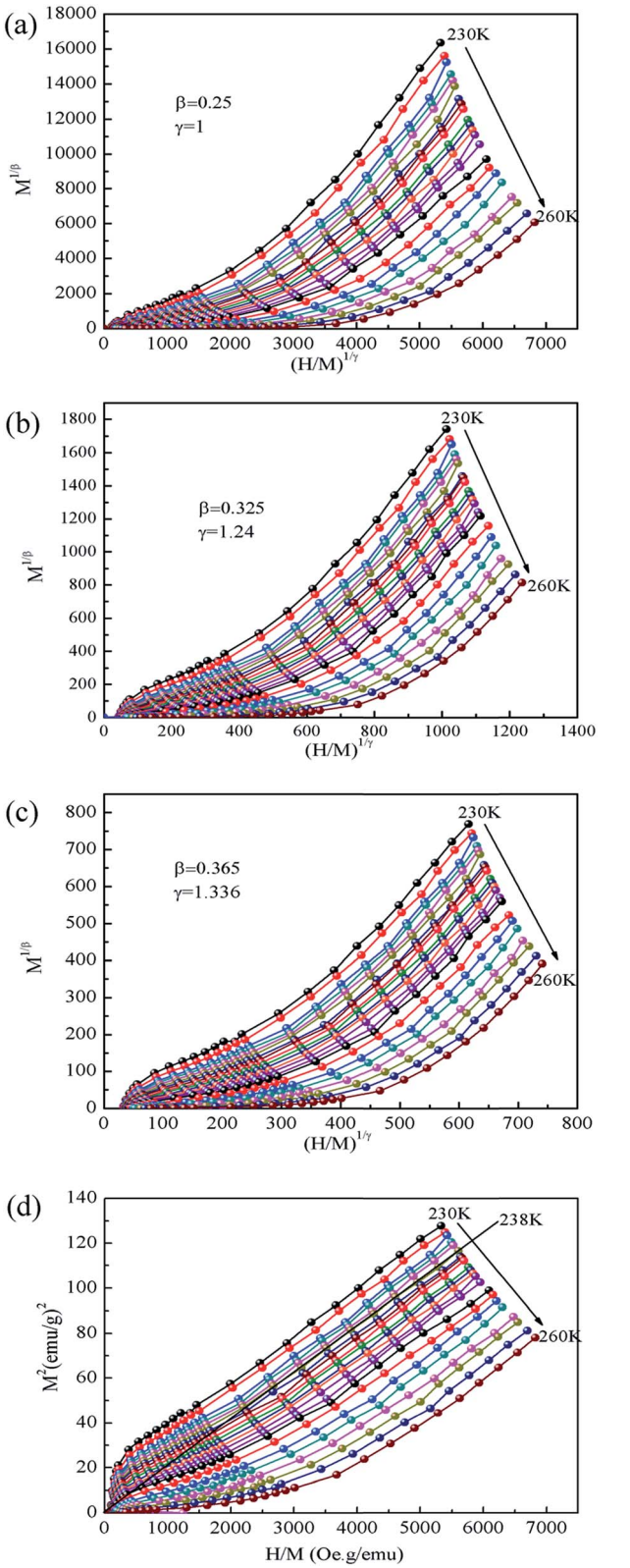

Fig. 5 Arrott plot isotherms of $M^{1/\beta}$ *vs.* $(H/M)^{1/\gamma}$: (a) tricritical mean-field theory ($\beta = 0.25$, $\gamma = 1$), (b) 3D Ising model ($\beta = 0.325$, $\gamma = 1.24$), (c) 3D Heisenberg model ($\beta = 0.365$, $\gamma = 1.336$), (d) mean-field theory ($\beta = 0.5$, $\gamma = 1$).

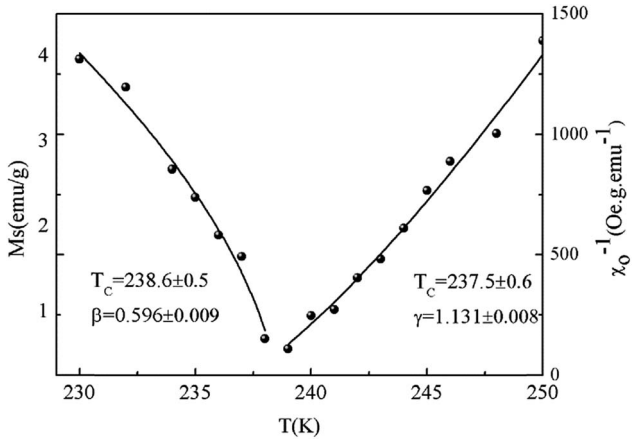

Fig. 6 Temperature as a function of the spontaneous magnetization M_s (left circles) and the inverse initial susceptibility χ_0^{-1} (right circles) along with the fitting curves based on the power laws (solid lines).

shown in the Fig. 7b. It proves the critical exponents are suitable for the FM–PM transition in the $La_{0.5}Ca_{0.5}MnO_3$ nanowires bundles and the curies temperature could be determined to be 238 K accurately.

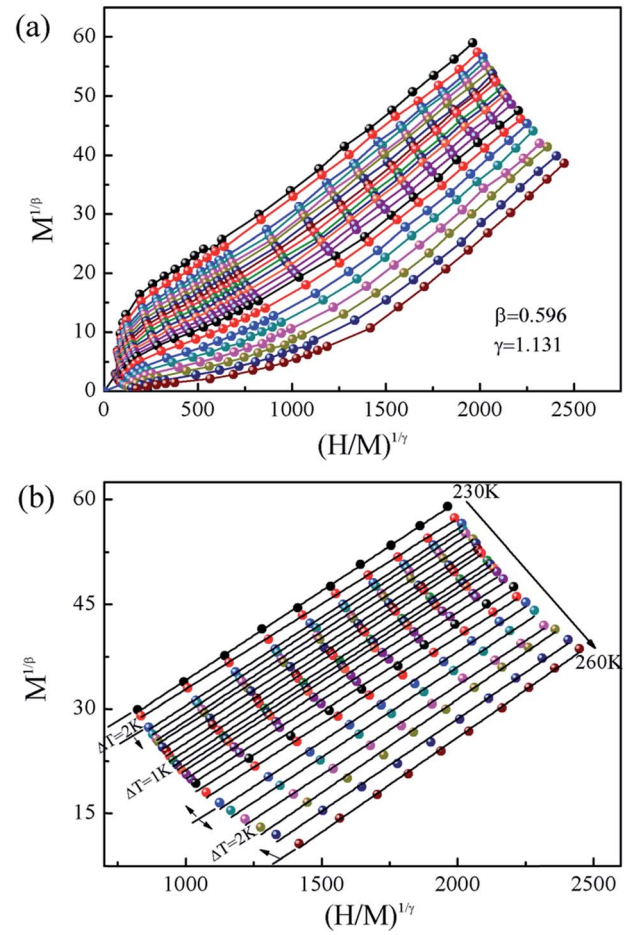

Fig. 7 (a) Modified Arrott plot of $M^{1/\beta}$ *vs.* $(H/M)^{1/\gamma}$ with $\beta = 0.596$, $\gamma = 1.131$. (b) $M^{1/\beta}$ *vs.* $(H/M)^{1/\gamma}$ Arrott plot in the high field 1–6 T region and the fitting lines (solid lines).

According to the eqn (3), the third critical exponent δ can be determined. The isothermal magnetization at $T_c = 238$ K is shown in Fig. 8 and the insert picture shows the plot with ln–ln scale. The ln(M) as a function of ln(H) yield range with the slope $1/\delta$, then, the $\delta = 2.99 \pm 0.05$ is obtained. Besides according to the statistical theory, these critical exponents of β, γ and δ satisfy the Widom scaling relation:[43]

$$\delta = 1 + \gamma/\beta \quad (4)$$

$\delta = 2.90 \pm 0.04$ was calculated from the relation. Obviously, the value of $\delta = 2.99 \pm 0.05$ obtained from the inset of Fig. 7 agrees well with the data calculated from the wisdom scaling relation. In the critical region, according to the prediction of the scaling equation, the magnetic equation can be written as

$$M(H,|\varepsilon|) = \varepsilon^{\beta} f_{\pm}(H/|\varepsilon|^{\beta+\gamma}) \quad (5)$$

where $f_{\pm}$ are regular functions with f_+ for $T > T_c$ and f_- for $T < T_c$. The $M(H,\varepsilon)\varepsilon^{-\beta}$, as a function of $H\varepsilon^{-(\beta+\gamma)}$, yields two universal curves for $T > T_c$ and $T < T_c$, respectively. The experimental data fall on two curves as shown in Fig. 9, which is in agreement with the scaling theory, indicating that the present exponents are reasonably accurate and unambiguous.

For the relation of the field dependence of magnetic entropy change in a magnetic system with a second-order phase transition, Oesterreicher and parker ever proposed a universal relational expression: $|\Delta S_M| \propto H^n$, where $n = 2/3$,[44] $|\Delta S_M|$ is the maximum of magnetic entropy change around T_c.

However, due to the inappropriateness in some soft magnetic amorphous alloys with $n = 2/3$, Franco *et al.* modified the relation mentioned above and re-provided a serious of new relations named magnetocaloric effect scaling laws.[45] One of the most necessary relations of the scaling laws is

$$n = 1 + (\beta - 1)/(\beta + \gamma) \quad (6)$$

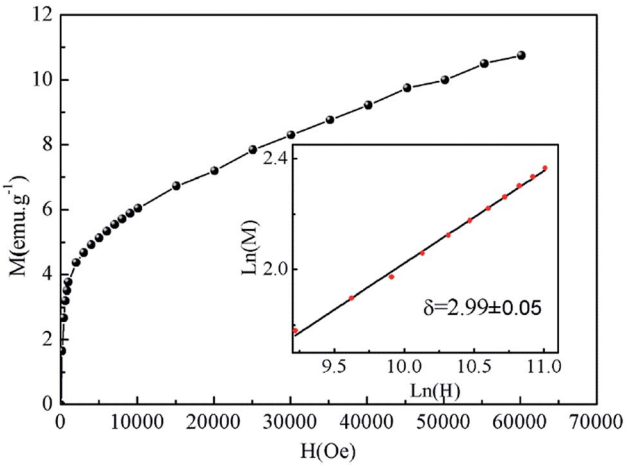

Fig. 8 Isothermal M *vs.* H plot of $La_{0.5}Ca_{0.5}MnO_3$ at $T_c = 238$ K; the inset shows the same plot in ln–ln scale and the solid line is the fitting straight line following eqn (3).

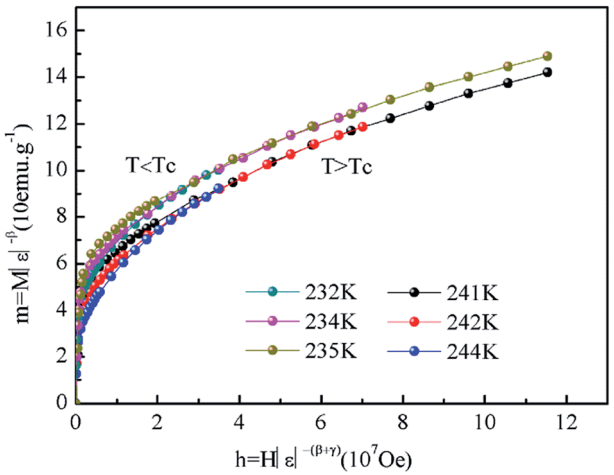

Fig. 9 Scaling plots blow and above T_c using β and γ determined by modified critical exponent.

here, we attempt to calculate the critical exponent of β and γ according to the eqn (6) and (4). In order to obtain the value of n, we calculated the magnetic entropy change according to conventional method firstly.[46] Fig. 10a shows the temperature dependence of $-\Delta S$ under different applied field changes from 1 T to 6 T. The relation of $|\Delta S_M|$ *versus* H is presented in Fig. 10b. The value of n is determined to be $n = 1.03 \pm 0.01$. Based on the obtained n and δ, the new values of $\beta = 1.10 \pm 0.04$ and $\gamma = 2.2 \pm 0.1$ can be obtained. Thus, a new Arrott plot was redrawn with the obtained β and γ (not shown here). As a result, the plot shows unexpected unparallel lines, which demonstrated the unsuitable of magnetocaloric effect scaling laws on $La_{0.5}Ca_{0.5}MnO_3$ nanowires bundles material. Therefore, we believe that the magnetocaloric effect scaling laws have no reliability for the nano-meter system.

Based on the results above, the critical exponents are similar to the mean-field model ($\beta = 0.50$, $\gamma = 1.0$ and $\delta = 3.0$) which holds if the exchange interaction is long-range type.[39,47–49] It can be observed that the critical exponents have some deviations from the mean-field theory. Physically, β describes how the ordered moment grows below T_c and γ describes the divergence of the magnetic susceptibility at T_c. In this nano-system, the obtained $\beta = 0.596 \pm 0.009$ is higher than common value β, indicating that there is a slower increase of the ordered moment than usual ferromagnets, which can be interpreted by the large surface and interface in nanoscale materials providing more disordered spin magnetic moments. $\gamma = 1.131 \pm 0.008$ is between the value of mean-field model and 3D Heisenberg model, indicating a higher curvature in the $M(H)$ curve. There are two reasonable hypothesis for these unexpected critical behaviors: first one, in nanoscale materials, the magnetic influence from the disorder magnetic state is high as surface effect become more prominent in nanograins. The ordered arrangement nanowires bundles provide large surface and interface that enable the domination of disordered magnetic state of the surface sites and affects the spin-lattice coupling in manganese perovskites.[50] In this situation, the decrease of particles' size leads to the inconsistent critical exponent between the actual and theoretical. The second one is the critical

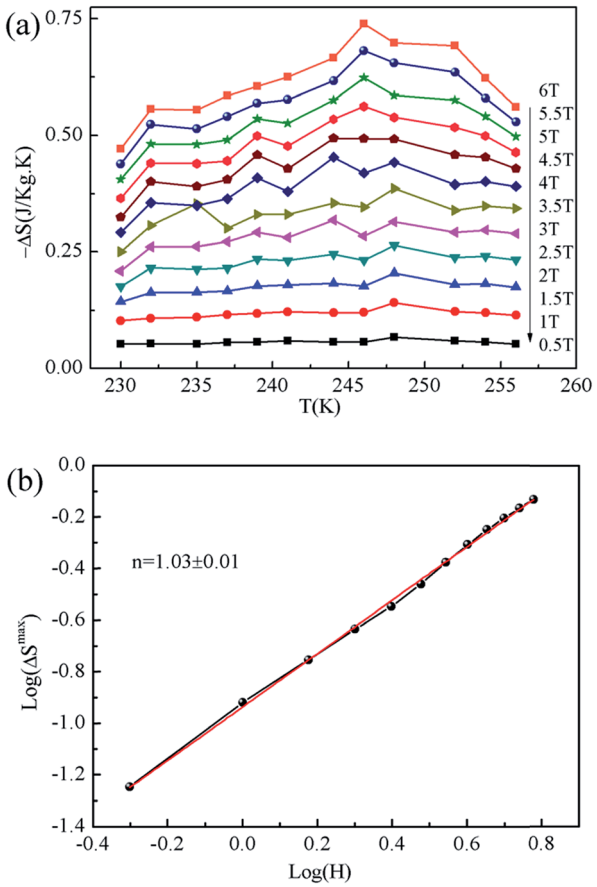

Fig. 10 (a) Temperature dependence of the magnetic entropy changes $-\Delta S$ under different external magnetic fields. (b) The maximal magnetic entropy change $|\Delta S_M|$ *vs.* H on log–log scale and the red line is the fitting curve.

transition theories were developed in bulk system[42] which may be not good for nano system. In addition, the magnetic entropy change shown in Fig. 10a is much lower than those in bulk materials.[51] The magnetic entropy is defined by the ordering degree of magnetic moments under external magnetic field. The magnetic entropy change $|\Delta S|$ is known to increase monotonically with magnetic field strengthening. It is harder to reach magnetic moments order under external magnetic field for nanoscale materials compared with corresponding bulk materials due to the high surface disorder, which gives interpretations for the lower magnetic entropy for nano-materials. There is an unexpected phenomenon that the $|\Delta S|$ has an almost linear relation with the external field as shown in Fig. 10. The parameter $n = 1.03 \pm 0.01$ was higher than those observed in other bulk materials.[52] The higher n value found in the nanocrystalline manganites can be attributed to their sensitivity to the magnetic fields which was few mentioned in the past literatures.[53]

Conclusions

In summary, the $La_{0.5}Ca_{0.5}MnO_3$ nanowires bundles were synthesized by hard template method. The critical properties of the perovskite manganite were studied using the isothermal

magnetization around Curie point T_c. Furthermore, the reliability of the modified critical exponents were proved based on Widom scaling relation and single scaling equation. It is found the exponents have some deviations from the mean-field model and the critical parameters don't obey the magnetization entropy scaling theory in this system, which can be attributed to the surface disorders or unsuitability of the theory in nano-system. Further investigation is necessary to clarify the strong discrepancy of the reported critical exponents.

Acknowledgements

The research was funded by National Natural Science Foundation of China (51402276 and 51202235) and Foundation of Science and Technology Department of Zhejiang Province (No. 2010R50016, 2014C31125). We also thank High Magnetic Field Laboratory, Chinese Academy of Sciences, for support.

Notes and references

1 E. O. Wollan and W. C. Koehler, *Phys. Rev.*, 1955, **15**, 545–563.
2 P. G. Radaelli, *Phys. Rev. B: Condens. Matter Mater. Phys.*, 1997, **55**, 3015–3023.
3 M. J. Zhi, G. W. Zhou, Z. L. Hong, J. Wang, R. Gemmen, K. Gerdes, A. Manivannan, D. L. Ma and N. Q. Wu, *Energy Environ. Sci.*, 2011, **4**, 139–144.
4 Y. M. Choi, M. C. Lin and M. L. Liu, *Angew. Chem., Int. Ed.*, 2007, **46**, 7214–7219.
5 F. Teng, W. Han, S. H. Liang, B. Gaugeu, R. L. Zong and Y. F. Zhu, *J. Catal.*, 2007, **250**, 1–11.
6 Y. Tian, D. R. Chen and X. L. Jiao, *Chem. Mater.*, 2006, **18**, 6088–6090.
7 Q. L. He, T. T. Yuan, S. Y. Wei and Z. H. Guo, *J. Mater. Chem. A*, 2013, **1**, 13064–13075.
8 Z. H. Guo, L. L. Henry, V. Palshin and E. J. Podlaha, *J. Mater. Chem.*, 2006, **16**, 1772–1777.
9 X. L. Chen, S. Y. Wei, C. Gunesoglu, J. H. Zhu, C. S. Southworth, L. Y. Sun, A. B. Karki, D. P. Young and Z. Guo, *Macromol. Chem. Phys.*, 2010, **211**, 1775–1783.
10 Q. L. He, T. T. Yuan, S. Y. Wei, N. Haldolaarachchige, Z. P. Luo, D. P. Young, A. Khasanov and Z. H. Guo, *Angew. Chem., Int. Ed.*, 2012, **51**, 8842–8845.
11 C. Zener, *Phys. Rev.*, 1951, **82**, 403–405.
12 S. H. Liang, F. Teng, G. Bulgan and Y. F. Zhu, *J. Phys. Chem. C*, 2007, **111**, 16742–16749.
13 B. Seyfi, M. Baghalha and H. Kazemian, *Chem. Eng. J.*, 2009, **148**, 306–311.
14 R. Pinedo, I. R. de Larramendi, D. Ji de Aberasturi, I. G. de Muro, A. T. Aguayo and J. I. Ruiz de Larramendi, *J. Mater. Chem.*, 2011, **21**, 10273–10276.
15 T. Zhang, C. G. Jin, T. Qian, X. L. Lu, J. M. Bai and X. G. Li, *J. Mater. Chem.*, 2004, **14**, 2787–2789.
16 D. Zhu, H. Zhu and Y. H Zhang, *J. Phys.: Condens. Matter*, 2002, **14**, L519–L524.
17 T. Tajiri, H. Deguchi, S. Kohiki, M. Mito, S. Takagi, M. Mitome, Y. I. Murakami and A. Kohno, *J. Phys. Soc. Jpn.*, 2008, **77**, 074715.
18 Z. H. Wang, T. H. Ji, Y. Q. Wang, X. Chen, R. W. Li, J. W. Cai, J.-R. Sun, B. G. Shen and C. H. Yan, *J. Appl. Phys.*, 2000, **87**, 5582–5584.
19 A. Carretero-Genevrier, J. Gázquez, J. C. Idrobo, J. Oró, J. Arbiol, M. Varela, E. Ferain, J. Rodríguez-Carvajal, T. Puig, N. Mestres and X. Obradors, *J. Am. Chem. Soc.*, 2011, **133**, 4053–4061.
20 P. ękała, V. Drozd, J. F. Fagnard and P. Vanderbemden, *J. Alloys Compd.*, 2010, **507**, 350–355.
21 J. N. Huang, Y. H. Cao, X. Zhang, Y. T. Li, J. Guo, S. Y. Wei, X. F. Peng, T. D. Shen and Z. H. Guo, *AIP Adv.*, 2015, **5**, 097183.
22 D. L. Leslie-Pelecky, *Chem. Mater.*, 1996, **8**, 1770–1783.
23 A. Biswas, I. Das and C. Majumdar, *J. Appl. Phys.*, 2005, **98**, 124310.
24 N. S. Bingham, P. Lampen, M. H. Phan, T. D. Hoang, H. D. Chinh, C. L. Zhang, S. W. Cheong and H. Srikanth, *Phys. Rev. B: Condens. Matter Mater. Phys.*, 2012, **86**, 064420.
25 H. Baaziz, A. Tozri, E. Dhahri and E. K. Hlil, *Solid State Commun.*, 2015, **208**, 45–52.
26 A. P. Ramirez, *J. Phys.: Condens. Matter*, 1997, **9**, 8171.
27 J. M. D. Coey, M. Viret and S. von Molnaír, *Adv. Phys.*, 1999, **48**, 167–293.
28 D. Kim, B. Revaz, B. L. Zink and F. Hellman, *Phys. Rev. Lett.*, 2002, **89**, 227202.
29 C. S. Hong, W. S. Kim and N. H. Hu, *Phys. Rev. B: Condens. Matter Mater. Phys.*, 2001, **63**, 092504.
30 B. I. Belevtsev, G. A. Zvyagina, K. R. Zhekov, I. G. Kolobov, E. Y. Beliayev, A. S. Panfilov, N. N. Galtsov, A. I. Prokhvatilov and J. Fink Finowicki, *Phys. Rev. B: Condens. Matter Mater. Phys.*, 2006, **74**, 054427.
31 R. I. Zainullina, N. G. Bebenin, V. V. Ustinov, Y. M. Mukovskii and D. A. Shulyatev, *Phys. Rev. B: Condens. Matter Mater. Phys.*, 2007, **76**, 014408.
32 C. V. Mohan, M. Seeger, H. Kronmüller, P. Murugaraj and J. Maier, *J. Magn. Magn. Mater.*, 1998, **183**, 348–355.
33 M. Hazzez, N. Ihzaz, M. Boudard and M. Oumezzine, *Phys. B*, 2015, **468–469**, 39–44.
34 G. Iniama, P. de la Presa, J. M. Alonso, M. Multigner, B. I. Ita, R. Cortés-Gil, M. L. Ruiz-González, A. Hernando and J. M. Gonzalez-Calbet, *J. Appl. Phys.*, 2014, **116**, 113901.
35 P. G. Radaelli, D. E. Cox, M. Marezio, S.-W. Cheong, P. E. Schiffer and A. P. Ramirez, *Phys. Rev. Lett.*, 1995, **75**, 4488–4491.
36 A. Das, P. D. Babu, S. Chatterjee and A. K. Nigam, *Phys. Rev. B: Condens. Matter Mater. Phys.*, 2004, **70**, 224404.
37 M. Pękała, V. Drozd, J. F. Fagnard and P. Vanderbemden, *J. Alloys Compd.*, 2010, **507**, 350–355.
38 D. Y. Zhao, Q. S. Huo, J. L. Feng, B. F. Chmelka and G. D. Stucky, *J. Am. Chem. Soc.*, 1998, **120**, 6024–6036.
39 I. Walha, H. Ehrenberg, H. Fuess and A. Cheikhrouhou, *J. Alloys Compd.*, 2007, **433**, 63–67.
40 A. Arrott and J. E. Noakes, *Phys. Rev. Lett.*, 1967, **19**, 786–789.
41 B. K. Banerjee, *Phys. Lett.*, 1964, **12**, 16.

42 H. E. Stanley, *Introduction to Phase Transitions and Critical Phenomena*, Oxford University Press, London, 1971.
43 B. Widom, *J. Chem. Phys.*, 1964, **41**, 1633.
44 H. Oesterreicher and F. T. Parker, *J. Appl. Phys.*, 1984, **55**, 4334–4338.
45 V. Franco, A. Conde, J. M. Romero-Enrique and J. SBlázquez, *J. Phys.: Condens. Matter*, 2008, **20**, 285207.
46 J. Y. Fan, L. S. Ling, B. Hong, L. Pi and Y. H. Zhang, *J. Magn. Magn. Mater.*, 2009, **321**, 2838–2841.
47 A. K. Pramanik and A. Banerjee, *Phys. Rev. B: Condens. Matter Mater. Phys.*, 2009, **79**, 214426.
48 S. N. Kaul, *J. Magn. Magn. Mater.*, 1985, **53**, 5–53.
49 M. E. Fisher, S. K. Ma and B. G. Nickel, *Phys. Rev. Lett.*, 1972, **29**, 917–920.
50 M. Kumaresavanji, C. T. Sousa, A. Pires, A. M. Pereira, A. M. L. Lopes and J. P. Araujo, *Appl. Phys. Lett.*, 2014, **105**, 083110.
51 M. Quintero, S. Passanante, I. Irurzun, D. Goijman and G. Polla, *Appl. Phys. Lett.*, 2014, **105**, 152411.
52 J. Y. Fan, L. Pi, L. Zhang, W. Tong, L. S Ling, B. Hong, Y. G. Shi, W. C. Zhang, D. Lu and Y. H. Zhang, *Appl. Phys. Lett.*, 2011, **98**, 072508.
53 M. Pękała, *J. Appl. Phys.*, 2010, **108**, 113913.